JOURNAL OF AIRCRAFT
Vol. 33, No. 1, January–February 1996

Vortex Ingestion in a Diffusing S-Duct Inlet

B. J. Wendt*
Modern Technologies Corporation, Middleburg Heights, Ohio 44130
and
B. A. Reichert†
Kansas State University, Manhattan, Kansas 66506

An experimental study of the effects of an ingested vortex on the flowfield of a diffusing S-duct inlet model is reported. Three test conditions vary by the location of where the vortex enters the model. For each test condition two different S-duct configurations are examined, a baseline S-duct and an S-duct with an array of surface-mounted vortex generators. The data taken consist of duct inlet and exit cross-plane surveys of velocity and total pressure and surface flow visualization. The data are compared to identical S-duct data taken in the absence of an ingested vortex. The ingested vortex is observed to have a strong influence on the S-duct flowfield, but only when the vortex trajectory is near the region of flow separation that exists in the baseline S-duct. The ingested vortex at this location reduces the extent of flowfield separation inside the baseline duct and promotes stronger crossflow of both the baseline duct and the duct with vortex generators. This enhanced crossflow also strengthens the vortices shed from the vortex generators. The other ingested vortex locations are found to produce little effect on the flowfield of the duct, with or without vortex generators.

Nomenclature

A	=	duct cross-sectional area perpendicular to the centerline
C_{p0}	=	total pressure coefficient
D	=	duct cross-sectional diameter
p	=	static pressure
p_0	=	total pressure
R	=	duct centerline radius of curvature
r	=	cross-plane radial coordinate
s	=	distance along S-duct centerline
x, y, z	=	Cartesian coordinates
ϕ	=	cross-plane polar angle

Subscripts

ref	=	reference conditions, at S-duct inlet
1, 2	=	stations at the S-duct inlet and exit

Introduction

AN initially uniform airstream enters an aircraft inlet and is routed to the engine face. Inlet performance, in terms of total pressure recovery and total pressure distortion, is degraded by flow phenomena originating within the duct. Internally generated distortion and recovery losses have been documented for a variety of inlet ducts. Relatively little information exists on inlet duct flow problems originating from nonuniform upstream conditions. An important type of upstream nonuniformity is a trailing vortex that has been ingested into the inlet. Such a vortex may be shed, e.g., from a forward component of the airframe during a high angle-of-attack maneuver.

In a recent computational study by Anderson[1] the effects of an ingested vortex on the flowfield within an F/A-18 inlet duct were examined. Anderson observed that the vortex trajectory within the duct behaves as though the flowfield were inviscid, and that for some values of vortex strength and location the ingested vortex negates the beneficial flow control effects provided by vortex generators installed on the duct surface.

The objective of the present study is to experimentally explore the effects of an ingested vortex on the flowfield within a diffusing S-duct. Two different configurations of the diffusing S-duct are considered, the baseline S-duct, and the same duct with an array of surface mounted vortex generators.

The flow features of the baseline configuration were explored in studies by Vakili et al.[2] and Wellborn et al.[3] Strong cross-stream pressure gradients developed by duct curvature give rise to secondary flows. Secondary flows, combined with an increasing cross-sectional area and adverse pressure gradient, result in a three-dimensional boundary-layer separation and a pair of counter-rotating axial vortices. These vortices produce total pressure distortion at the duct exit and contribute to the flow blockage that reduces the total pressure recovery of the duct.

Our recent experimental work[4] has shown that S-duct distortion may be significantly reduced and the total pressure recovery increased if vortex generators are used to counter or redirect the secondary flows near the duct surface. Boundary-layer flow separation is eliminated in the duct and the counter-rotating vortices are weakened, thereby reducing their deleterious effects on the flowfield. Of the eight different vortex generator arrays tested in Ref. 4, the configuration that produced the best total pressure recovery and the least distortion was used in this study.

The results for three different conditions of ingested vortex are reported here. The ingested vortex conditions vary by the location of where the vortex enters the S-duct. In the first condition, the center of the ingested vortex coincides with the centerline of the inlet cross plane. In the second condition, the center of the ingested vortex is near the duct surface in the location where strong secondary flows initiate boundary-layer separation. In the third condition, the center of the ingested

Presented as Paper 94-2811 at the AIAA/ASME/SAE/ASEE 30th Joint Propulsion Conference, Indianapolis, IN, June 27–29, 1994; received Aug. 30, 1994; revision received June 16, 1995; accepted for publication Aug. 12, 1995.

*Research Engineer, 7530 Lucerne Drive, Islander Two, Suite 100. Member AIAA.

†Assistant Professor, Department of Mechanical Engineering. Senior Member AIAA.

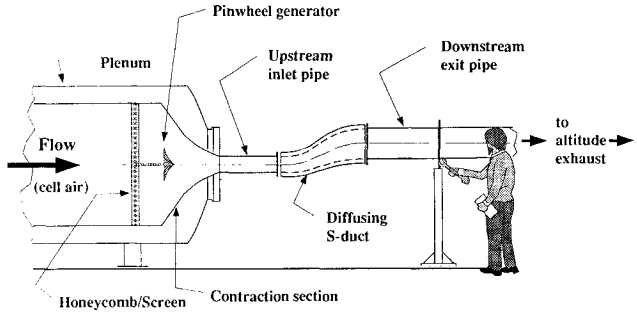

Fig. 1 Test section region of the IFMF showing the approximate mounting location of the ingested vortex generator pinwheel.

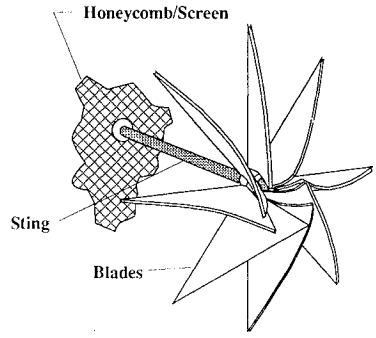

Fig. 2 Ingested vortex generator pinwheel.

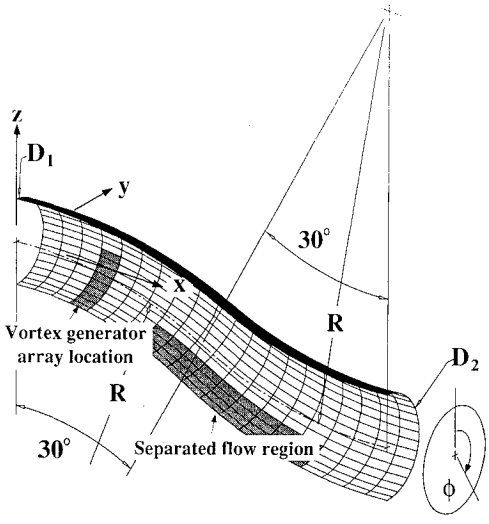

Fig. 3 Geometry of the diffusing S-duct.

vortex is near the duct surface opposite that of the second condition. Measurements of flow angularity, transverse velocity, and total pressure at the upstream cross plane aid in characterizing the ingested vortex initial strength, structure, and position.

For each condition of ingested vortex, a baseline S-duct and an S-duct with an array of vortex generators is tested. The data presented for each condition include total pressure and transverse velocity fields acquired at duct inlet and exit cross planes and surface flow visualization. The results are compared with data without ingested vortex, acquired in the previous baseline S-duct study[3] and S-duct with vortex generator study.[4]

Experimental Facilities and Procedures

Facility Flow Conditions

Experimental measurements of the duct flowfield were made at NASA Lewis Research Center using the Internal Fluid Mechanics Facility (IFMF). This facility was designed to support the research of a variety of internal flow configurations and is described in detail by Porro et al.[5] The facility is schematically illustrated in Fig. 1. As shown in Fig. 1, smooth circular pipes of appropriate diameter are attached upstream and downstream of the S-duct to produce (in the absence of the pinwheel described later) a uniform incoming flow and a smooth, continuous condition for flow exiting the duct. The lengths of the upstream and downstream pipes are each $3.75D_1$. The duct inlet Mach number is 0.6 for all experimental test conditions and measurements. The inlet boundary-layer thickness is approximately 4% of the duct inlet diameter and the Reynolds number, based on inlet diameter, is 2.6×10^6.

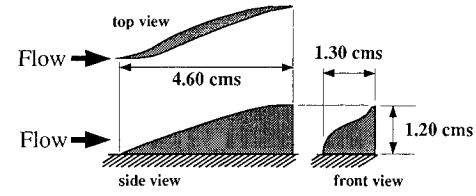

Fig. 4 Geometry of the tapered-fin vortex generators.

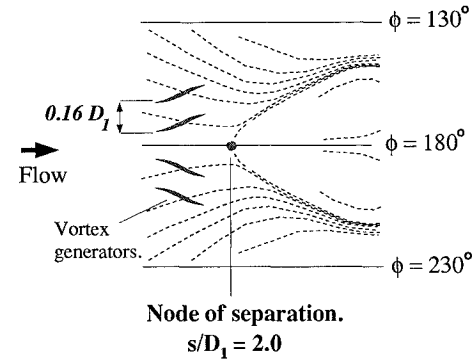

Fig. 5 Vortex generators are positioned to counter the converging flow near the node of separation.

The ingested vortex is generated with a nonrotating eight-bladed pinwheel. The triangular blades of the pinwheel were cut from a one-eighth-in. sheet of aluminum rolled to an i.d. of 61.0 cm. The eight blades were welded to a single aluminum hub or ring to form the pinwheel pattern, as is illustrated in Fig. 2. When looking upstream, the ingested vortex is seen to rotate in a counterclockwise direction. The pinwheel was mounted on a sting anchored to the honeycomb-screen combination of the facility plenum section. The sting and pinwheel extended downstream about 35.6 cm into the contraction section of the tunnel as indicated in Fig. 1. The location of the ingested vortex is varied by changing the pinwheel position.

Baseline Diffusing S-Duct

One symmetric half of the diffusing S-duct examined in this study is shown in Fig. 3. This duct is geometrically similar to the duct tested in Ref. 2 and is identical to the duct studied in Refs. 3 and 4. The duct centerline is defined by two circular 30-deg arcs with an identical radius of curvature, $R = 102.1$ cm. Both arcs lie within the xz plane as shown in Fig. 3. The cross-sectional shape of the duct perpendicular to the centerline is circular. When discussing locations within the duct, axial location will refer to distance to cross-stream planes measured along the duct centerline and normalized by the duct inlet diameter s/D_1. Position within cross-stream planes is specified by ϕ, measured from the vertical in a positive clockwise direction as shown in Fig. 3, and the radial distance from the centerline r. The diameter of the cross-section varies with the axial location as follows:

$$\frac{D}{D_1} = 1 + 3\left(\frac{D_2}{D_1} - 1\right)\left(\frac{s/D_1}{5.23}\right)^2 - 2\left(\frac{D_2}{D_1} - 1\right)\left(\frac{s/D_1}{5.23}\right)^3 \quad (1)$$

Table 1 Summary of test cases

S-duct configurations	Upstream boundary conditions: No ingested vortex	Ingested vortex on duct centerline	Ingested vortex near duct wall at $\phi \approx 180°$	Ingested vortex near duct wall at $\phi \approx 0°$
Baseline	1	3	5	7
Vortex generators	2	4	6	8

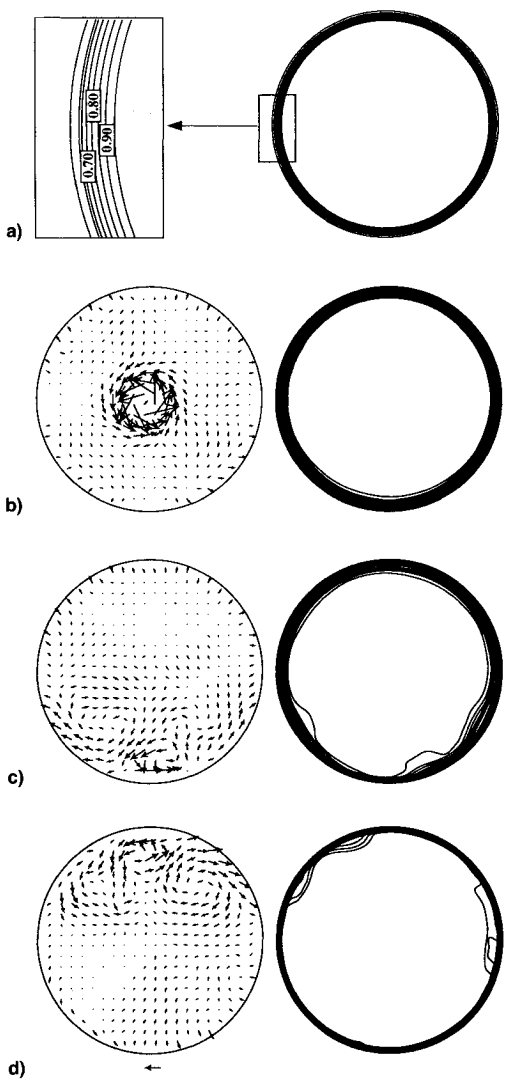

Fig. 6 Transverse velocity and total pressure results at the duct inlet plane. Test cases a) 1 and 2, b) 3 and 4, c) 5 and 6, and d) 7 and 8.

In Eq. (1) and Fig. 3, $D_1 = 20.4$ cm is the diameter at the duct inlet and $D_2 = 25.1$ cm is the diameter at the duct exit. This provides an exit to inlet area ratio of $A_2/A_1 = 1.52$. The offset of the duct resulting from the centerline curvature is $1.34D_1$, and the length of the duct measured along the centerline is $5.23D_1$. The geometric plane of symmetry runs parallel to the duct centerline and intersects the angular positions of $\phi = 0$ and 180 deg. The approximate streamwise location of boundary-layer separation in the baseline duct is indicated in Fig. 3. Also shown is the approximate mounting position used for vortex generators in the duct.

Diffusing S-Duct with Vortex Generators

The vortex generators used are illustrated in Fig. 4. These devices are similar to the tapered fin first examined in the report of Schubauer and Spangenberg.[6] Each vortex generator will produce a single trailing axial vortex when its leading edge is aligned with the flow as indicated in Fig. 4. The height of the vortex generators tested was on the order of the flowfield boundary-layer thickness.

The basis for flow control using arrays of these devices can be understood from flow visualization data obtained in the baseline diffusing S-duct. Figure 5 illustrates surface flow visualization results, shown as dashed lines, obtained by using oil dots. Upstream of the axial location of flow separation ($s/D_1 = 2.0$) in the angular range $80 \leq \phi \leq 280$ deg, the boundary-layer flow is converging strongly toward the line of flowfield symmetry $\phi = 180$ deg. Continuity forces these converging flows away from the duct surface near $\phi = 180$ deg. This motion initiates the naturally occurring pair of counter-rotating vortices observed at the duct exit for flow without installed vortex generators. Also, the converging flow of low momentum fluid thickens the boundary layer near $\phi = 180$ deg and reduces its ability to withstand streamwise adverse pressure gradients, contributing to flow separation. The vortex generators are mounted in arrays to counter this converging flow, as shown in Fig. 5. An array of four vortex generators with a lateral spacing of $0.16D_1$ was used in this study. This vortex generator array eliminated boundary-layer separation and produced the least flow distortion and greatest total pressure recovery of the eight configurations tested in Ref. 4.

Measurement Techniques

The primary set of measurements consists of inlet and exit cross-plane surveys of the mean three-dimensional velocity field and total pressure. The inlet survey cross plane was located a distance of $0.5D_1$ upstream of the S-duct inlet. The data were acquired by making nine radial traverses across the inlet diameter with a single five-hole probe. Each radial traverse consisted of 32 equally spaced measurements. Measurement resolution along the radial axis was $\Delta r/D_1 = 0.031$ and $\Delta\phi = 20$ deg circumferentially. The exit survey plane was located a distance of $0.5D_1$ downstream of the S-duct exit. The velocity and total pressure data were acquired with a rake probe consisting of 10 equally spaced and independently calibrated five-hole probe tips. The rake probe was traversed radially and circumferentially to acquire data at 720 locations. Measurement resolution on the radial axis was $\Delta r/D_2 = 0.025$ and $\Delta\phi = 10$ deg circumferentially. More information on the geometry, construction, and calibration of the five-hole probe rake used in this study can be found in the report of Wendt and Reichert.[7]

In addition to the velocity and pressure field surveys, visualization of the near-surface duct flow was conducted using a fluorescent oil dot technique. The flow pattern revealed by the oil dots was photographed under uv illumination. These patterns were then transferred (by contact) to absorbent paper so that two-dimensional tracings of the flow pattern could be rendered.

Results and Discussion

Total pressure data are plotted in terms of the following nondimensional pressure coefficient:

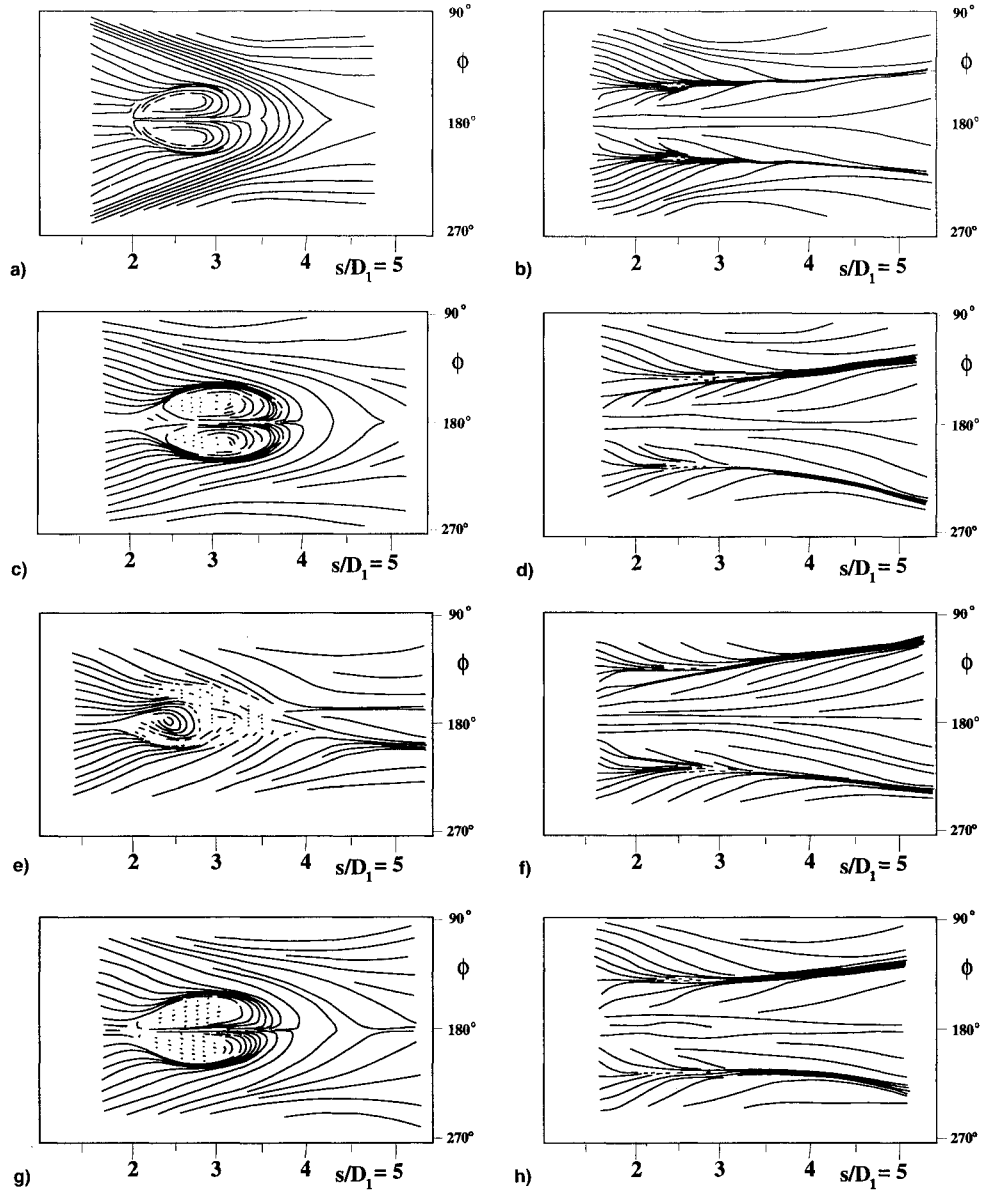

Fig. 7 Surface flow visualization results. Test cases a) 1, b) 2, c) 3, d) 4, e) 5, f) 6, g) 7, and h) 8.

$$C_{p0} = \frac{p_0 - p_{\text{ref}}}{p_{0,\text{ref}} - p_{\text{ref}}} \tag{2}$$

The reference value of total pressure is the freestream total pressure, which is nominally equal to atmospheric pressure. The reference value of static pressure is the freestream static pressure, which is determined by averaging the simultaneously recorded values of 18 static pressure taps spaced 20 deg apart around the duct inlet.

Transverse velocity and total pressure results originate from five-hole probe pressure measurements acquired with an electronically scanned transducer system. The transducer's manufacturer states a measurement uncertainty of ±0.05 kPa. Uncertainty in the pressure measurement data is used to derive velocity and total pressure result uncertainty following the procedure outlined by Reichert and Wendt.[8] Uncertainty in flow angle measurement is ±0.3 deg, in either pitch or yaw component, and the corresponding uncertainty in transverse velocity magnitude is approximately ±0.5% of the cross-plane-averaged total velocity magnitude. Total pressure coefficient uncertainty is approximately ±1%.

Table 1 summarizes the test cases covered for this study. Two different S-duct configurations are charted against four upstream boundary conditions, making a total of eight test cases. The test case numbers in Table 1 are used in this section to discuss results. Test cases 1 and 2 are without the ingested vortex and are included for comparison. Test cases 3–8 are the ingested vortex cases.

Upstream Results

Figure 6 illustrates the upstream results for each condition of ingested vortex. The velocity scale is provided by the reference vector at the bottom of Fig. 6. This vector represents one-tenth the cross-plane-averaged total velocity magnitude. Figure 6a is a contour plot of total pressure at the inlet cross plane in the absence of the ingested vortex (test cases 1 and 2). The inset shows the uniform boundary layer present here.

Figure 6b illustrates the transverse velocity and total pressure data for the ingested vortex on the duct centerline (test cases 3 and 4). A strong, coherent vortical structure is evident from the transverse velocity data, which has been interpolated from the radial survey grid to the Cartesian grid shown. Maximum flow angles are approximately 10 deg. Vortex flow effects are confined to a sector roughly 10 cms in diameter and centered on $r = 0$. The ingested vortex has no apparent effect on the total pressure field in Fig. 6b.

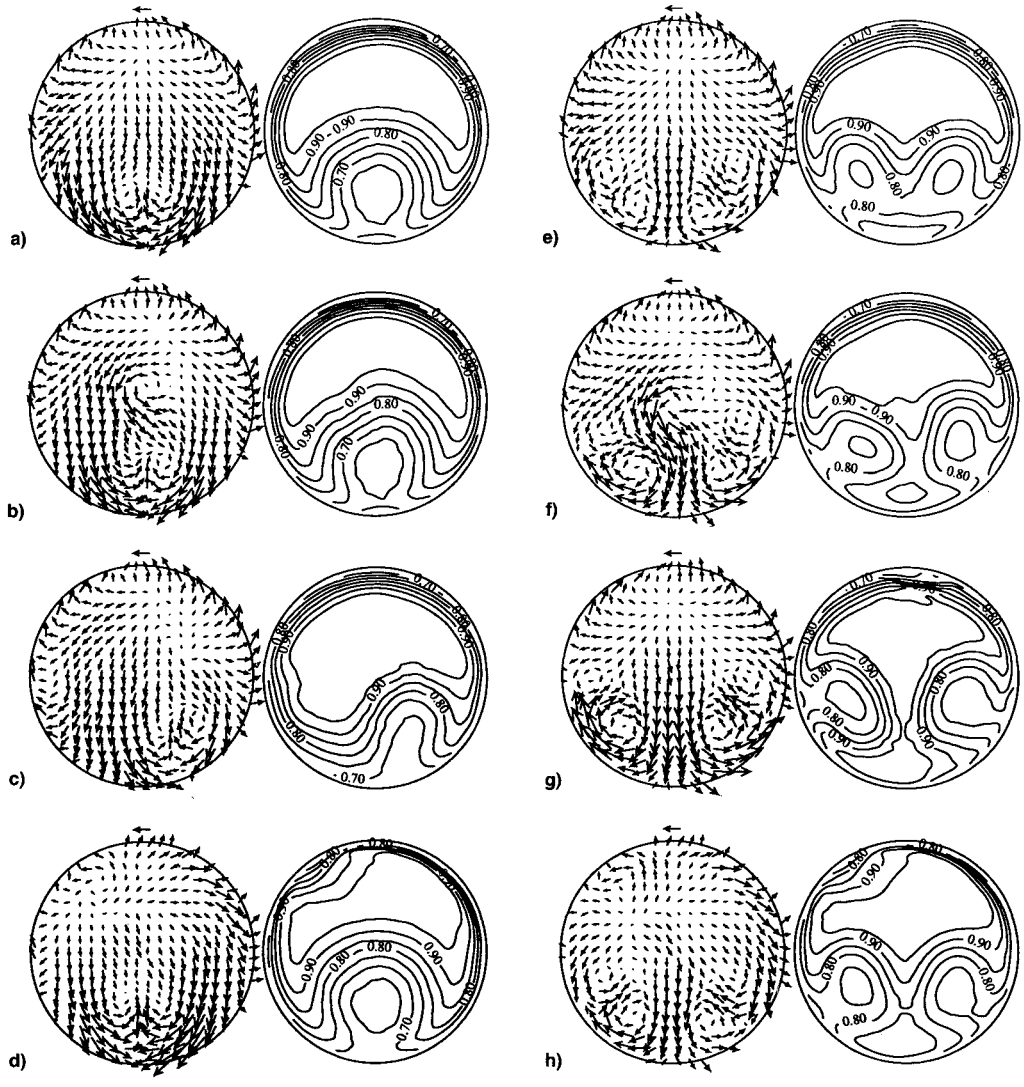

Fig. 8 Transverse velocity and total pressure results at the duct exit plane. Test cases a) 1, b) 3, c) 5, d) 7, e) 2, f) 4, g) 6, and h) 8.

Figures 6c and 6d illustrate the off-centerline locations of the ingested vortex. Figure 6c presents the transverse velocity and total pressure results for test cases 5 and 6, Fig. 6d for test cases 7 and 8. The velocity data show a grouping of three distorted vortices for both of these locations. The center vortex (a counterclockwise vortex, closest to the wall) is the strongest of the three. This vortex is the pinwheel-generated vortex. The additional vortices in the flowfield are most likely the result of an interaction between the pinwheel-generated vortex and the upstream contraction surface boundary layer. Corresponding distortions in the boundary-layer profiles are apparent in the total pressure contours of Figs. 6c and 6d.

S-Duct Results

Figure 7 illustrates the surface flow visualization results obtained inside the diffusing S-duct. In each figure the flow is from left to right. Figures 7a and 7b represent test cases 1 and 2. The vortical region of flow separation is clearly evident in Fig. 7a. In the absence of the ingested vortex the baseline flowfield possesses mirror image symmetry through the line $\phi = 180$ deg. This is also true for the diffusing S-duct with a symmetric array of vortex generators installed as depicted in Fig. 5. Note the absence of separated flow in Fig. 7b.

Figures 7c, 7e, and 7g are the surface flow visualization results for the baseline S-duct with ingested vortex (test cases 3, 5, and 7, respectively). The effect of the ingested vortex is seen to be strongest in test case 5. Flow stagnation on the surface is still evident over the axial range $2 < s/D_1 < 4$ indicating flow separation, but the structure of this region is now different from reference test case 1. The mirror image symmetry of the vortical separation is absent, and a smaller, more concentrated, region of vortical flow appears on the surface, centered on the line $\phi = 180$ deg. Downstream, in the angular range $180 < \phi < 270$ deg, the surface streak lines converge and trail off towards higher values of ϕ creating an asymmetric pattern in contrast to Fig. 7a. Crossflow created by the near-wall proximity of the ingested vortex is the probable cause of this effect. The flow visualization results for test cases 3 and 7 illustrate that these conditions of ingested vortex have little influence on the surface flow features of the duct in the region of flow separation.

Figures 7d, 7f, and 7h are the surface flow results for the S-duct with an array of vortex generators (test cases 4, 6, and 8, respectively). Qualitatively, these present the same surface flow features seen in Fig. 7b. The divergence of the two patterns of converging streak lines (from $\phi = 180$ deg) results when the crossflow created by the vortex generator array redirects the naturally occurring crossflow as discussed in the Introduction. The divergence of the two streak line patterns in Fig. 7f is somewhat greater than that observed in the other vortex generator test cases. We also have evidence, from Fig. 7e, that this condition of ingested vortex is creating a crossflow pattern sweeping down from $\phi = 180$ deg towards higher values of ϕ. Thus, the ingested vortex is observed to enhance the

crossflow created by that portion of the vortex generator array installed over $\phi > 180$ deg.

Downstream Results

Figure 8 illustrates the exit plane transverse velocity and total pressure results for all test cases. As with the upstream velocity data, the transverse velocity scale is provided by a reference vector above each plot. The interpretation of this vector is the same as before.

The transverse velocity field of Fig. 8a clearly shows the naturally occurring pair of counter-rotating up-flow vortices. The term up flow refers to the convective action of the flow between the vortex cores. Low momentum fluid from the boundary-layer region of the duct flowfield is convected up into the core flow by the vortices. The resulting distortion of the total pressure field is depicted in Fig. 8a. The flowfield possesses mirror image symmetry with respect to a line passing through the duct walls at the circumferential positions of $\phi =$ 0 and 180 deg.

The ingested vortex is clearly visible in the transverse velocity field of Fig. 8b. The effects of the ingested vortex on the total pressure field in test case 3 is minimal, however. In the transverse velocity field of Fig. 8c, no vortex structure identifiable as an ingested vortex is visible, but we clearly see the convective influence of this vortex. Note the shift in the position of the naturally occurring up-flow vortices, to the right of center. This shift, due to the convective influence of the counter-clockwise ingested vortex, is also apparent in the total pressure contours. Note also that the region of low momentum fluid is reduced somewhat in size.

The other location of the ingested vortex, depicted in Fig. 8d, does not influence the exit plane results to the same extent exhibited in Fig. 8c. A small vortex structure, identified as the ingested vortex, is evident at the 10 o'clock position near the wall in the transverse velocity field of Fig. 8d. The influence of the ingested vortex on the total pressure contours here is seen as a distortion in the boundary layer on the wall opposite to the low momentum region created by the naturally occurring vortices.

Figure 8e illustrates the transverse velocity and total pressure results at the exit cross plane of the S-duct with an array of vortex generators and no ingested vortex (test case 2). In the transverse velocity field we observe four vortices; the exterior vortices are the naturally occurring pair discussed earlier, and the interior vortices are created by the upstream array of vortex generators. Note the strong downflow now present on the line of flowfield symmetry. The effect on the total pressure contours is to split the region of low momentum fluid, seen in Fig. 8a, into two smaller regions displaced to either side of the symmetry line.

Figures 8f–8h illustrate the effect of the ingested vortex on this flowfield. In the transverse velocity field of Fig. 8f we clearly see the presence of the centrally located ingested vortex. The corresponding total pressure contours indicate that this vortex is having little effect on these results. Figure 8g verifies what we deduced from flow visualization inside the duct: the ingested vortex is enhancing the effects of the vortex generator array on the flowfield. Note that the two interior vortices (due to the generators) and the region of downflow on the previous symmetry line are now much stronger than that observed in Fig. 8e. Figure 8h is similar to the pattern depicted in Fig. 8e, except for the small distortion in the boundary layer on the wall opposite the location of the vortices. This result is analogous to that occurring in the baseline duct for this condition of ingested vortex (Fig. 8d).

Summary

An experimental study of the effects of an ingested vortex on the flowfield of a diffusing S-duct is reported. The vortex is generated through the use of a stationary pinwheel device mounted upstream of the diffusing S-duct. Three test conditions vary the location of where the vortex enters the duct inlet cross plane. For each condition of ingested vortex, a baseline S-duct and an S-duct with an array of vortex generators is tested. The data taken consist of duct inlet and exit cross-plane surveys of velocity and total pressure and duct surface flow visualization. The data acquired in this test are compared to identical S-duct data taken in the absence of the ingested vortex.

In the first condition the ingested vortex enters on the center of the duct inlet cross plane. Measurements of flow angle, transverse velocity, and total pressure at both inlet and exit cross planes indicate a strong central vortex, with maximum flow angles of approximately 10 deg. When compared to identical results taken in the absence of the ingested vortex, little effect on the inlet and exit cross-plane total pressure contours and near surface flow behavior was evident.

In the second condition, the ingested vortex trajectory is near the region of flow separation that exists in the baseline S-duct. This location of the ingested vortex promotes stronger regions of transverse flow in the duct exit plane. Profiles of total pressure and surface flow features differ considerably from test cases without the ingested vortex. The strength of the vortices shed from the array of vortex generators is enhanced by the convective influence of the ingested vortex.

In the third condition, the ingested vortex is near the duct wall opposite that of the second condition. When compared to identical results taken in the absence of the ingested vortex, little effect on the inlet and exit cross-plane total pressure contours and near surface flow behavior was evident.

Acknowledgments

We are grateful for the help and insight provided by W. Darby, F. Forsyth, B. Gronski, W. Hingst, C. Wasserbauer, and K. Zaman.

References

[1]Anderson, B. H., "The Aerodynamic Characteristics of Vortex Ingestion for the F/A-18 Inlet Duct," AIAA Paper 91-0130, Jan. 1991.

[2]Vakili, A. D., Wu, J. M., Liver, P., and Bhat, M. K., "Experimental Investigation of Secondary Flows in a Diffusing S-Duct," Univ. of Tennessee Space Inst. TR UTSI 86/14, Tullahoma, TN, Jan. 1984.

[3]Wellborn, S. R., Reichert, B. A., and Okiishi, T. H., "An Experimental Investigation of the Flow in a Diffusing S-Duct," AIAA Paper 92-3622, July 1992; also NASA TM 105809, Aug. 1992.

[4]Reichert, B. A., and Wendt, B. J., "Improving Diffusing S-Duct Performance by Secondary Flow Control," AIAA Paper 94-0365, Jan. 1994; also NASA TM 106492, Jan. 1994.

[5]Porro, A. R., Hingst, W. R., Wasserbauer, C. A., and Andrews, T. B., "The NASA Lewis Research Center Internal Fluid Mechanics Facility," NASA TM 105187, Sept. 1991.

[6]Schubauer, G. B., and Spangenburg, W. G., "Forced Mixing in Boundary Layers," *Journal of Fluid Mechanics*, Vol. 8, No. 1, 1960, pp. 10–31.

[7]Wendt, B. J., and Reichert, B. A., "A New Algorithm for Five-Hole Probe Calibration and Data Reduction and Its Application to a Rake-Type Probe," *Fluid Measurement and Instrumentation Forum—1993*, edited by R. Gore, T. Morrow, and G. Jones, American Society of Mechanical Engineers, New York, 1993, pp. 29–35.

[8]Reichert, B. A., and Wendt, B. J., "Uncertainty of Five-Hole Probe Measurements," *Fluid Measurement and Instrumentation 1994*, edited by T. B. Morrow, G. L. Morrison, and R. A. Gore, American Society of Mechanical Engineers, New York, 1994, pp. 39–44.